



**HAL**  
open science

## Self-propulsion of inverse Leidenfrost drops on a cryogenic bath

Anaïs Gauthier, Christian Diddens, Rémi Proville, Detlef Lohse, Devaraj van Der Meer

► **To cite this version:**

Anaïs Gauthier, Christian Diddens, Rémi Proville, Detlef Lohse, Devaraj van Der Meer. Self-propulsion of inverse Leidenfrost drops on a cryogenic bath. *Proceedings of the National Academy of Sciences of the United States of America*, 2019, 116 (4), pp.1174-1179. 10.1073/pnas.1812288116 . hal-03555654

**HAL Id: hal-03555654**

**<https://hal.science/hal-03555654v1>**

Submitted on 3 Feb 2022

**HAL** is a multi-disciplinary open access archive for the deposit and dissemination of scientific research documents, whether they are published or not. The documents may come from teaching and research institutions in France or abroad, or from public or private research centers.

L'archive ouverte pluridisciplinaire **HAL**, est destinée au dépôt et à la diffusion de documents scientifiques de niveau recherche, publiés ou non, émanant des établissements d'enseignement et de recherche français ou étrangers, des laboratoires publics ou privés.

# Self-propulsion of inverse Leidenfrost drops on a cryogenic bath

Anais Gauthier<sup>a,1</sup>, Christian Diddens<sup>a,b</sup>, Rémi Provaille<sup>c</sup>, Detlef Lohse<sup>a,d</sup>, and Devaraj van der Meer<sup>a</sup>

<sup>a</sup>Physics of Fluids group and Max Planck Center Twente. Mesa + Institute and Faculty of Science and Technology, J.M. Burgers Centre for Fluid Dynamics and Max Planck Center Twente for Complex Fluid Dynamics. University of Twente, P.O. Box 217 7500 AE Enschede, The Netherlands; <sup>b</sup>Department of Mechanical Engineering, Eindhoven University of Technology, P.O. Box 513, 5600 MB Eindhoven, The Netherlands; <sup>c</sup>INSERM, Neurocentre Magendie, Physiopathologie de la plasticité neuronale, U1215, 33077, Bordeaux, cedex, France; <sup>d</sup>Max Planck Institute for Dynamics and Self-Organization, 37077 Göttingen, Germany

This manuscript was compiled on June 3, 2020

**When deposited on a hot bath, volatile drops are observed to stay in levitation: the so-called Leidenfrost effect. Here, we discuss drop dynamics in an inverse Leidenfrost situation where room-temperature drops are deposited on a liquid nitrogen pool, and levitate on a vapor film generated by evaporation of the bath. In the seconds following deposition, we observe that the droplets start to glide on the bath along a straight path, only disrupted by elastic bouncing close to the edges of the container. Initially at rest, these self-propelled drops accelerate within a few seconds and reach velocities on the order of a few cm/s before slowing down on a longer time scale. They remain self-propelled as long as they are sitting on the bath, even after freezing and cooling down to liquid nitrogen temperature. We experimentally investigate the parameters that affect liquid motion, and propose a model, based on the experimentally and numerically observed (stable) symmetry breaking within the vapor film that supports the drop. When also the film thickness and the cooling dynamics of the drops are modeled, the variations of the drop velocities can be accurately reproduced.**

drops | self-propulsion | Leidenfrost | liquid nitrogen bath | gliding

When deposited on a hot solid, volatile drops can levitate over a cushion of their own vapor - a phenomenon extensively described by J.G. Leidenfrost (1) in the 18th century. Being insulated from the substrate by a vapor layer, the Leidenfrost drops have a lifetime of the order of a few minutes (2). Moreover, in absence of friction, they do not only glide at the slightest inclination but also bounce (3), jump (4) or oscillate (5), rich dynamics (6) that make the control of such drops a problem. On solid substrates, addition of a well-chosen texture can efficiently guide drops, as first demonstrated by Linke *et al.* (7): asymmetric textures can redirect the vapor flow below the liquid (8), which generates self-propulsion. This is used to efficiently guide or even entrap levitating drops (9–11) or solids (12). However, controlling drop motion seems more complex on deformable substrates such as liquid baths, where Leidenfrost levitation also occurs (13–16, 18). The liquid surface, resisting the weight of the drops is notably deformed (19, 20), but this does not impact drop mobility, as there is no contact drag (21, 22). The suspended drops were observed to sometimes glide for tens of seconds (14, 16, 18, 23, 24), and have to be trapped to perform some measurements (13).

In this paper, we consider the dynamics of ethanol or silicone oil droplets deposited on a liquid nitrogen bath, in an "inverse" Leidenfrost scenario (25) where vapor generated by the bath maintains drops above the pool. We show that, contrary to what is seen on solid substrates, a spontaneous symmetry breaking occurs that leads to a self-propelling state - a phenomenon that we investigate experimentally. Using

simulations, we demonstrate that the movements arise from a difference in the film thickness between the front and the back of the drop, which we use to model the gliding dynamics.

**Experiment.** Liquid nitrogen is a cryogenic liquid with boiling temperature of  $-196^{\circ}\text{C}$  and low latent heat of vaporization  $L_v = 2 \times 10^5 \text{ J/kg}$ . Its evaporations is fast enough so that, when a drop at ambient temperature approaches a nitrogen bath, the generated vapor cushion can maintain the drop in the Leidenfrost state (16, 23). As opposed to more usual Leidenfrost situations (1–3) where vapor is produced by the levitating objects, here vapor comes from the bath so that the drops keep a constant radius  $R$  over time. However, the drops continuously cool down (below their freezing point), until their temperature reaches that of the bath, which sometimes causes their sinking (16, 23). To avoid ebullition within the pool, we followed Adda-Bedia *et al.* (16) by placing the central bath (with diameter  $D = 7.6 \text{ cm}$ ) at the center of a sacrificial bath of liquid nitrogen, itself inside an homemade polystyrene cryostat. As schematized in Figure 1a, the sacrificial bath is continuously boiling, which maintains a nitrogen atmosphere in the box. The residual evaporation of the central bath (at approximately  $0.1 \text{ L/h}$ , due to radiative heat exchanges at the top) does not disturb the liquid surface that remains perfectly still. Drops of ethanol (density  $\rho = 789 \text{ kg/m}^3$ , specific heat  $c_p = 2400 \text{ J/kg/K}$  at  $20^{\circ}\text{C}$ ) or silicone oil ( $\rho = 930 \text{ kg/m}^3$ ,  $c_p = 1600 \text{ J/kg/K}$ ) with radii  $R$  ranging from  $0.65 \text{ mm}$  to  $1.8 \text{ mm}$  are formed from calibrated needles and released  $\simeq 1 \text{ cm}$  above the bath surface. The chosen liquids have low

## Significance Statement

An inverse Leidenfrost state can happen when ambient temperature drops are deposited on liquid nitrogen, as the bath evaporation generates a vapor film that maintains drops in levitation. Contrary to what is seen on solids, drops levitating on a cryogenic liquid exhibit counter-intuitive dynamics: they are spontaneously self-propelled (and glide in straight lines) and keep levitating even after cooling down to a temperature equal to that of the bath. This spontaneous self-propulsion in a cryogenic environment - that last for tens of minutes - can be seen as an efficient way to freeze and further transport biological materials (such as cells or proteins) or chemicals without contamination or risk of heat degradation.

A.G., D. vdM. and D.L. designed research, A.G. performed experiments, A.G. and R.P. analysed data, C.D. did the simulations and A.G. led the writing.

The authors declare no conflict of interest.

<sup>1</sup>To whom correspondence should be addressed. E-mail: a.e.gauthier@utwente.nl

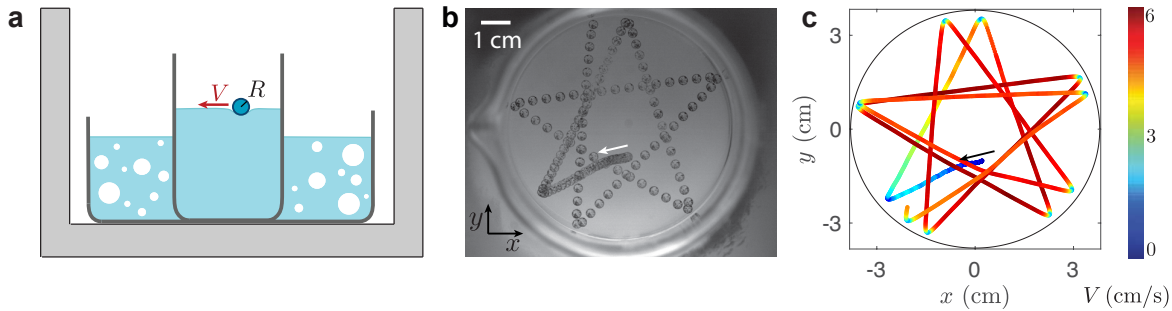


**Fig. 1.** **a.** Schematic of the experimental setup: a drop with radius  $R$  is deposited on a liquid nitrogen bath. To avoid ebullition of the central bath, it is placed in a styrofoam box, and maintained at the center of a sacrificial bath whose evaporation maintains a nitrogen atmosphere in the box. Drop trajectory and velocity  $V$  are recorded from the top. **b.** Chronophotography of the successive positions (separated by 80 ms) of an ethanol drop ( $R = 1.5$  mm) seeded with particles. The white arrow indicates the initial position and movement of ethanol. **c.** Trajectory of the center of mass of the same drop in the  $x$ - $y$  plane in a longer time interval. The color indicates the drop velocity, varying from  $V = 0$  (dark blue) to  $V = 6$  cm/s (dark red).

freezing temperatures ( $< -100^\circ\text{C}$ ), which limits their freezing in the needles. Moreover, such drops keep a smooth spherical shape when they freeze, which does not always happen for water drops (17). Once released, the drops, denser than liquid nitrogen (density  $\rho_N = 808$  kg/m<sup>3</sup>), initially sink; but nitrogen evaporation generates a buoyant force that almost immediately pushes them back to the surface, where they remain (23). Drop trajectory and velocity  $V$  are recorded from the top at typically 125 fps, and the origin of time  $t$  is chosen as soon as Leidenfrost levitation happens.

Figure 1b shows the first 15 seconds of motion of an ethanol drop with radius  $R = 1.5$  mm seeded with particles - two successive images are separated by 80 ms. The white arrow indicates the initial position and direction of the drop. Ethanol, initially at rest, slowly accelerates and starts hovering on the bath in straight lines. This regular movement is only disturbed by almost perfect reflections close to the edges of the beaker, producing a remarkable star-shaped trajectory. The droplet is initially subjected to strong internal motion (that can be seen on Movie S1) that vanishes as the liquid cools down and freezes (which happens between the second and the third bouncing) - with no visible impact on its movement. As visible in Movie S1, the surface of the bath remain still as the drop hovers it. The drop velocity  $V$ , of a few centimeters per second, is small enough not to generate any stationary wake (22).

In Figure 1c, the trajectory of the drop center of mass is plotted: the position  $(x,y) = (0,0)$  is the center of the beaker and the black circle corresponds to the edge of the bath. The color code indicates the drop velocity  $V$ . Initially 0 (dark blue),  $V$  increases up to 6 cm/s (dark red) after the 4<sup>th</sup> bouncing, and then slowly diminishes to reach 4 cm/s after the 13<sup>th</sup> bouncing. Interestingly, the propulsion mechanism is not disturbed by the successive rebounds: in the first instants, the drop keeps accelerating even after turning back close to the edge. The setting in motion of the drops is observed for every liquid tested (ethanol, silicone oil, propanol, butanol, pentanol, water), provided the drops were small and light enough to be supported by the liquid nitrogen bath. Depending on the first incident angle of the drop with the wall, trajectories vary from diagonals (for a perfectly normal incidence) to stars with varying number of branches - as in the SI Appendix, Fig.1 - up to triangles, pentagons and circles (for a tangent impact). Finally, it can be noted that self-propulsion is also seen for millimeter-sized particles (polyethylene spheres), although for

a much shorter duration. Similarly to frozen drops, the solid particles do not exhibit any rotational movement while gliding (as in Movie S2).

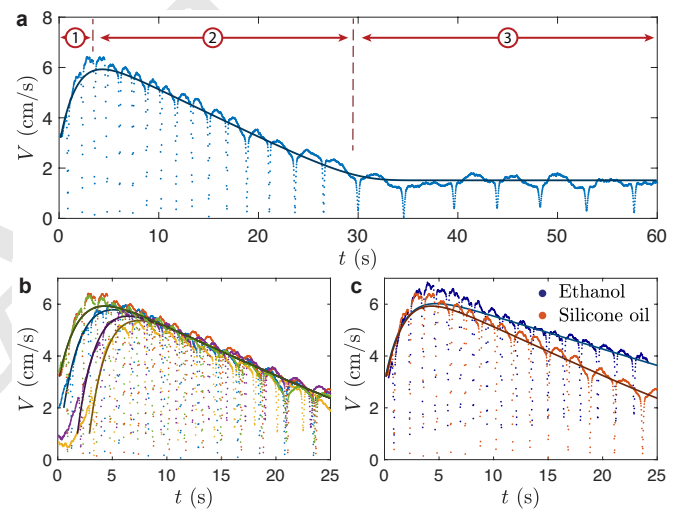


**Fig. 2.** **Drop velocity** **a.** Velocity  $V$  of a drop of silicone oil ( $R = 1.4$  mm) gliding on a liquid nitrogen bath, as a function of time  $t$ . The numbers mark the 3 phases of movement: acceleration, deceleration and constant velocity. The corresponding movie is Movie S3. **b.** Comparison of the velocity  $V(t)$  of 5 identical silicone oil drops deposited slightly differently on the bath. **c.** Velocity  $V(t)$  of ethanol ( $R = 1.4$  mm) deposited slightly differently on the bath. **c.** Velocity  $V(t)$  of ethanol (blue dots, specific heat  $c_p = 2400$  J/kg/K) and silicone oil drop (orange dots,  $c_p = 1600$  J/kg/K) with similar radius ( $R = 1.4$  mm) and initial velocity. In **a**, **b** and **c**, the darker lines are the numerical solution of Eq. 5, with identical prefactors  $\alpha = \beta = 15$ , and  $\Delta h = 1.45$   $\mu\text{m}$

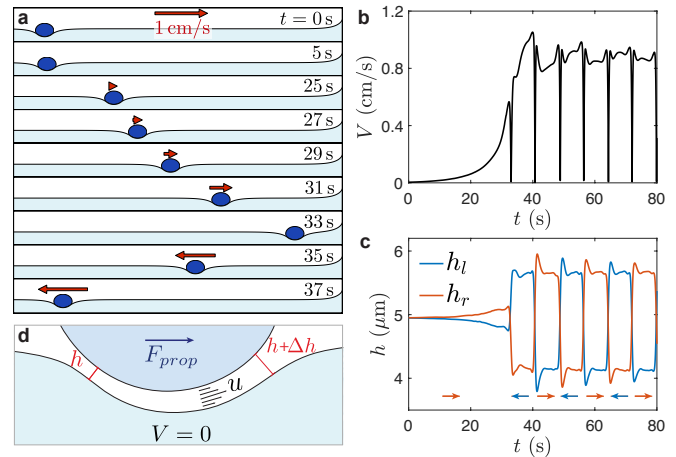
The velocity dynamics  $V(t)$  is even more intriguing. Figure 2a shows  $V(t)$  for a silicone oil drop ( $R = 1.4$  mm) as it glides on the bath (see also Movie S3). After falling from the needle, the drop sinks and resurfaces with an initial velocity  $V(t = 0) = 3.2$  cm/s, and immediately accelerates. The shape of  $V(t)$  results from the combination of two effects. First, at each rebound, the velocity  $V$  decreases and rises up again to the same value - indicating elastic bouncing. The drop bounces 23 times during its 60 s lifetime: each event can be distinguished individually in Fig. 2a. Second,  $V(t)$  exhibits very regular variations on a longer timescale (variations that are quite undisturbed by the repeated bounces) and that we call here the *velocity amplitude*  $V_A(t)$ .  $V_A$  is highlighted by the black line (which is the numerical solution of Eq. 5) and

249 can be decomposed in 3 phases, numbered on Fig. 2a: (1) An  
 250 *acceleration* phase (for  $0 < t < 5$  s) where the drop velocity  
 251 amplitude increases from  $V_A = 3.2$  cm/s to 6.5 cm/s. (2) A  
 252 *deceleration* phase (for  $5 < t < 30$  s) that lasts 5 times longer  
 253 than the acceleration, and during which  $V_A$  decreases linearly  
 254 with time. (3) A *constant velocity* phase ( $30 < t < 60$  s)  
 255 with  $V_A \simeq 2$  cm/s. This third phase can sometimes last  
 256 several minutes, until an outside event (a small movement of  
 257 the liquid surface or an encounter with a floating ice cristal)  
 258 makes the drop sink. The levitation time is much longer than  
 259 the expected Leidenfrost duration, which is of the order of  
 260 30 s for millimeter-sized drops initially at ambient temperature  
 261 (16). It can also be noticed that drop immersion after more  
 262 than 30 s hardly generates any boiling (see Movie S4), which  
 263 indicates that the particle temperature is then close to the  
 264 vaporization temperature of the bath.

265 Figure 2b shows 5 velocity plots (colored dots) obtained  
 266 by repeating the same experiment (silicone oil,  $R = 1.4$  mm)  
 267 but varying the height at which the drops are deposited. If  
 268 the velocity amplitudes of drops with identical initial velocity  
 269 perfectly overlap (as for the green and red curves), varying the  
 270 initial conditions impacts the acceleration phase. In particular,  
 271 it can be noted that sometimes (yellow and purple plots), the  
 272 drops do not accelerate immediately but exhibit an erratic  
 273 motion at low velocity ( $V < 1$  cm/s) for the first seconds before  
 274 starting to self-propel. Interestingly, this does not impact the  
 275 second phase of the drop movement (the deceleration) where  
 276 all  $V_A(t)$  plots perfectly overlap. Finally, Fig. 2c compares  
 277 the velocity profiles of ethanol and silicone oil with identical  
 278 radius  $R = 1.4$  mm and initial velocity. Contrary to Fig 2b,  
 279 changing the nature of the liquid affects the deceleration rate,  
 280 which is significantly (30%) lower for ethanol than for silicone  
 281 oil. However, varying the drops freezing temperature, or  
 282 preheating them hardly influences the velocity amplitude (see  
 283 the SI Appendix, Fig.2). We now aim to understand and  
 284 model the phenomena at the origin of the rich drop dynamics.  
 285

286 **Origin of self-propulsion.** A first insight on the cause of self-  
 287 propulsion is obtained through numerical simulation. Both  
 288 vapor and liquid flows are calculated in a 2d model system,  
 289 using a sharp-interface finite element method. A drop is  
 290 deposited at the center of a liquid nitrogen bath and the initial  
 291 vapor film is symmetric. As visible in Movie S5, the mesh  
 292 is made very fine below the drop - to resolve the thin gas  
 293 film - and coarser outside. For simplicity, thermal effects are  
 294 neglected and the bath evaporates at a constant rate of  $2.15$   
 295  $\text{g/s}^2$ . The motion of a drop with radius  $R = 1$  mm and viscosity  
 296  $\eta = 16$  mPa.s, as obtained numerically is presented in Fig.  
 297 3a: even if no pre-existing asymmetry is imposed, the droplet  
 298 spontaneously self-propels, as also visible in Movie S6. In Fig  
 299 3b, the drop velocity  $V$  is plotted as a function of time:  $V$   
 300 increases to finally reach a constant value  $V_A^* = 0.85 \pm 0.1$  cm/s.  
 301 Similarly to what is seen experimentally, the velocity amplitude  
 302 is not significantly impacted by the repeated drop about-turns  
 303 close to the edges of the bath.

304 Beyond a mere reproduction of the self-propulsion, the  
 305 simulation gives access to the details of the film thickness  
 306 and its variation with time, information difficult to obtain  
 307 experimentally. In figure 3c, the minimum film thicknesses  
 308 (measured at the neck) on the left side of the drop ( $h_l$ , in  
 309 blue) and on the right side ( $h_r$ , in red) are extracted from  
 310 the simulation and plotted as a function of time. While



311  
312  
313  
314  
315  
316  
317  
318  
319  
320  
321  
322  
323  
324  
325  
326  
327  
328  
329  
330  
331  
332  
333  
334  
335  
336  
337  
338  
339  
340  
341  
342  
343  
344  
345  
346  
347  
348  
349  
350  
351  
352  
353  
354  
355  
356  
357  
358  
359  
360  
361  
362  
363  
364  
365  
366  
367  
368  
369  
370  
371  
372

**Fig. 3.** a. Successive images extracted from the 2d-simulations. A drop with viscosity  $\eta = 16$  mPa.s and radius  $R = 1$  mm is deposited on an evaporating bath, and spontaneously self-propels. The corresponding movie is Movie S6. b. Drop velocity  $V$  as a function of time  $t$ . c. Difference in film thickness  $h$  between the left ( $h_l$ , in blue) and right part ( $h_r$ , in red) of the drop where the film is thinner. d. Model for the propulsion force: the film has a mean thickness  $h \ll R$ , and vapor is continuously escaping with a characteristic velocity  $u$ . The difference  $\Delta h \ll h$  in the film thickness changes the vapor distribution, generating a viscous propelling force  $F_{prop}$ , directed towards the larger opening.

initially,  $h_l$  and  $h_r$  are equal, they spontaneously diverge until a constant asymmetry  $\Delta h = |h_l - h_r| \simeq 1.5 \pm 0.1 \mu\text{m}$  is reached. Thus, Figure 3c gives essential indications on the origin of self-propulsion. First, comparison with Fig. 3b shows that the appearance of the asymmetry corresponds to the setting in motion of the drop. A geometrical asymmetry would indeed partially redirect the flow of vapor towards the larger opening, and thus generate a propelling force. In addition, the film is systematically thicker at the front ( $h_r$  when the drop moves to the right,  $h_l$  when it moves to the left). The drop follows the preferential direction of motion of the vapor, which indicates that the mechanism that causes self-propulsion is surely of viscous origin. Finally, it should be noted that the asymmetry spontaneously switches from left to right when the drop gets close to the liquid meniscus at the edge of the bath. While the direction of  $\Delta h$  changes, its amplitude is not impacted: the same asymmetric state consistently reappears. This strongly suggests that the symmetric film thickness is metastable, and that self-propulsion is generated by a spontaneous and constant symmetry breaking within the vapor film.

358  
359  
360  
361  
362  
363  
364  
365  
366  
367  
368  
369  
370  
371  
372

**Model.** The main result of the simulation is now used to model drop dynamics. As observed in the numerics, we assume a constant asymmetry with amplitude  $\Delta h$  in the film thickness  $h$  (with  $\Delta h \ll h$ ) between the front and the back of the drop. As illustrated in Fig. 3d, and similarly to what is seen on textured solids (7, 26), the asymmetry partially redirects the flow of vapor, which enable motion. The difference of viscous stresses between the front and the back generates a propelling force  $F_{prop}$  which can be estimated:  $F_{prop}$  is a fraction  $\Delta h/h$  of the total viscous force exerted on the bottom of the drop, varying as  $\eta_v \frac{u}{h} R^2$  (with  $\eta_v$  the viscosity of nitrogen vapor and  $u$  the typical velocity of the Poiseuille flow within the film), which gives  $F_{prop} \sim \frac{\Delta h}{h} \eta_v \frac{u}{h} R^2$ . This expression is simplified using lubrication theory: the pressure drop  $\Delta p$  within the vapor film scales as  $\Delta p \sim \eta_v \frac{u}{h^2} R$  and the overpressure in the film

373 sustains the drop, which implies  $\Delta p \sim \rho g R$  for drops smaller  
 374 than the capillary length (2, 16). These three expressions  
 375 combined give the following propelling force:

$$376 \quad F_{prop} \sim \rho g R^2 \Delta h, \quad [1]$$

377 which is similar to what is observed for uneven Leidenfrost  
 378 solids (26).  $F_{prop}$  dominates at the first instants of motion,  
 379 during acceleration; but as the drop velocity increases, the  
 380 friction force  $F_f$  gains importance. Our hypothesis is that its  
 381 dominant contribution also comes from the film: while gliding  
 382 (with velocity  $V$ ) the drop entrains vapor and its movement  
 383 creates a secondary Couette flow within the film, with a mean  
 384 velocity  $\propto V$ . This generates a viscous friction force that can  
 385 be written as:

$$386 \quad F_f \sim \eta_v \frac{V}{h} R^2. \quad [2]$$

387 The full calculation, (in a simplified situation) confirms this  
 388 argument and is given in the SI Appendix. The friction force  
 389 (inversely proportional to the film thickness  $h$ ) has the unusual  
 390 property of increasing with time. Indeed, as the drop cools  
 391 down, less and less nitrogen vapor is produced and the film  
 392 thins out. To fully determine  $F_f(t)$ , we then need to model  
 393  $h(t)$ . Calculations of the film thickness have been done with  
 394 a different purpose for levitating drops on solids (2), or on  
 395 hot baths (13), and in the inverse Leidenfrost state (16): we  
 396 follow a similar line of arguments here.

397 For drops in an inverse Leidenfrost scenario,  $h(t)$  arises  
 398 from two simultaneous processes: (i) vapor production and  
 399 escape and (ii) drop cooling dynamics. We give here the main  
 400 physical ingredients (a detailed calculation can be found in  
 401 the SI Appendix). (i) Due to the temperature difference  $\Delta T$   
 402 between the drop and the bath, heat diffuses through the  
 403 film and vaporises liquid nitrogen. The escaping vapor is  
 404 then confined below the drop, and lubrication generates an  
 405 overpressure that sustains the drop. For any given  $\Delta T$ , these  
 406 two elements give the following scaling law for  $h$ :

$$407 \quad h \sim \left( \frac{\eta_v \lambda \Delta T R}{\rho g \rho_v L_v} \right)^{1/4} \quad [3]$$

408 where  $\eta_v$ ,  $\rho_v$  and  $\lambda$  respectively denote the viscosity, density  
 409 and conductivity of the vapor,  $L_v$  the latent heat of vapor-  
 410 isation of liquid nitrogen,  $\rho$  drop density and  $g$  gravity. (ii)  
 411 Simultaneously, due to heat diffusion through the film, the  
 412 drop cools down. The rate of decrease of the drop internal  
 413 energy  $\rho R^3 c_p \frac{dT}{dt}$  (with  $c_p$  the drop specific heat) is equal  
 414 to the rate at which energy diffuses through the vapor film  
 415  $\lambda \Delta T / h R^2$ . Combined with Eq. 3, integration of this differ-  
 416 ential equation finally gives  $h(t)$ , which is found to decrease  
 417 linearly with time:

$$418 \quad h \sim h_0 (1 - t/\tau) \quad \text{with} \quad h_0 \sim \left( \frac{\eta_v \lambda \Delta T_0 R}{\rho g \rho_v L_v} \right)^{1/4} \quad [4]$$

$$419 \quad \text{and} \quad \tau \sim \frac{4 \rho R c_p h_0}{\lambda}.$$

420  $h_0$  is the initial film thickness: for millimeter-sized drops  
 421 and  $\Delta T_0 \simeq 200^\circ\text{C}$ ,  $h_0 \simeq 50 \mu\text{m}$ . This is in good agreement

422 with measurements done on solid substrates (2) or with the  
 423 results of numerical calculations (13) for drops on a bath. The  
 424 characteristic time  $\tau$  arises from the drop cooling dynamics:  
 425 it is the time needed for drops to cool down from ambient  
 426 temperature to liquid nitrogen temperature. For millimeter-  
 427 sized drops, this time is of the order of 20 s.

428 Using Eq.s 1, 2 and 4 we can finally model the dynamics  
 429 of the droplet. Writing  $m$  for the drop mass, Newton's second  
 430 law gives the following differential equation for the velocity  
 431 amplitude  $V_A(t)$ :

$$432 \quad m \frac{dV_A}{dt} = -\alpha \eta_v \frac{V_A}{h(t)} R^2 + \beta \rho g R^2 \Delta h \quad [5]$$

433 with  $\alpha$  and  $\beta$  numerical coefficients arising from geometrical  
 434 factors (respectively for  $F_f$  and  $F_{prop}$ ) which are not considered  
 435 in scaling laws. Since  $F_f$  and  $F_{prop}$  both originate from the  
 436 vapor flow within the film, we can assume that  $\alpha$  and  $\beta$  are  
 437 close. Thus, in the rest of the discussion, we will consider  
 438  $\alpha \simeq \beta$ , and the two fitting parameters in Eq. 5 are  $\alpha$  and  $\Delta h$ .  
 439 The temporal dependence of the velocity amplitudes  $V_A(t)$  is  
 440 simply deduced from Eq. 5 using a separation of times scales.  
 441 On the one hand,  $h(t)$  varies in a time  $\tau \simeq 20$  s while, on the  
 442 other hand, the characteristic time of the acceleration phase is  
 443  $\tau_{acc} \sim \rho R h / \eta_v \simeq 1$  s. Therefore, during the acceleration phase  
 444 the film thickness  $h(t)$  remains roughly constant, and Eq. 5 can  
 445 be approximated by a first-order linear differential equation.  
 446 Denoting  $V_{A0}$  the initial drop velocity,  $V_A(t)$  increases expo-  
 447 nentially, with  $V_A(t) = V_{A0} + (V_A^* - V_{A0})(1 - \exp(-t/\tau_{acc}))$ ,  
 448 until the drop reaches its terminal velocity  $V_A^*$ , obtained by  
 449 equalizing the propelling and friction forces (Eq. 1 and 2):

$$450 \quad V_A^*(t) = \frac{\rho g}{\eta_v} \Delta h h(t). \quad [6]$$

451 On a longer time scale, film thinning affects  $V_A^*(t)$  that de-  
 452 creases linearly with time (as  $h$  does, from Eq. 4) in a char-  
 453 acteristic time  $\tau$ . This model nicely reproduces the first 2  
 454 phases of the drop movement, as seen in figures 2b and c: the  
 455 darker lines are the numerical solution of Eq. 5, with the same  
 456 fitting parameters  $\alpha = 15$  and  $\Delta h = 1.45 \mu\text{m}$ . In figure 2b,  
 457 the collapse of the  $V_A(t)$  plots during the deceleration phase  
 458 is due to the drops reaching their terminal velocity, identical  
 459 for all five experiments. However, the nature of the liquid  
 460 affects the deceleration rate, as illustrated in Figure 2c. The  
 461 difference in deceleration rate between ethanol and silicone  
 462 oil is mainly due to a difference in the liquid specific heats  
 463  $c_p$ . Ethanol drops with  $c_p = 2400$  J/kg cool down in  $\tau \simeq$   
 464 43 s where silicone oil drops (with  $c_p = 1600$  J/kg) cool down  
 465 faster ( $\tau \simeq 30$  s); which directly impacts the slope of  $V_A^*(t)$ .

466 In addition, the amplitude of the asymmetry  $\Delta h$  causing  
 467 self-propulsion can be deduced from the velocity amplitude  
 468 dynamics. Figure 4a shows the best fit of  $V_A(t)$  obtained for  
 469 varying drop radii  $R$ : smaller drops have lower internal energy  
 470 and cool down faster, which is nicely reproduced by Eq 5. By  
 471 repeating systematically this experiment (with drop radius  
 472  $R$  varied between 0.64 and 1.8 mm) we plotted (in Fig. 4b)  
 473 the value of  $\Delta h$  giving the best fit as a function of  $R$ . More  
 474 specifically, we considered the second phase of drop dynamics,  
 475 where drops decelerate at a constant rate  $a$  (phase 2 in Fig  
 476 2a). The experimental measurement of  $a$  gives  $\Delta h$ , that is

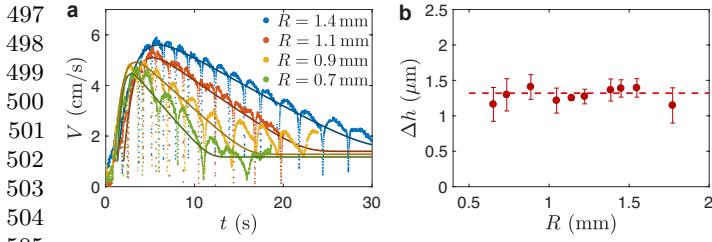


**Fig. 4.** **a.** Velocity  $V(t)$  of silicon oil drops with varying drop radius  $R$ . The darker lines are the solutions of Eq. 5 for each drop size. **b.** Amplitude of the asymmetry  $\Delta h$  deduced from the best fit of the drop deceleration.

expected to vary proportionally to  $a \frac{\eta_v \tau}{\rho g h_0}$ , as calculated from Eq. 6. In Figure 3c,  $\Delta h$  is found to be of the order of  $1 \mu\text{m}$ , which is consistent with our initial hypothesis of a small film deformation ( $\Delta h \ll h \simeq 50 \mu\text{m}$ ) and with the result of the numerical simulation. Remarkably,  $\Delta h$  remains constant over the range of drop radii we tested ( $0.64 \text{ mm} < R < 1.8 \text{ mm}$ ). This is quite different from what is seen for self-propelled uneven solids (26) where  $\Delta h \propto \sqrt{R}$ .

Incidentally, Eq. 5 explains why the drop does not rotate in the stable asymmetric state: reaching the terminal velocity, the propelling and friction forces balance, which implies - for an approximately spherical drop - that also the net torque on the drop balances, consistent with our observations.

**Self-propulsion of pool liquid and frozen drops.** Interestingly, liquid nitrogen drops deposited delicately on the liquid nitrogen bath can also levitate (without coalescing) for long periods of time, even if their temperature is the same as that of the bath. Similarly to hot drops, these cryogenic drops are self-propelled: Figure 5a shows successive positions (separated by 250 ms) of a liquid nitrogen drop with radius  $R = 1.8 \text{ mm}$  10 minutes after being deposited. As also seen in Movie S7, the drop has a regular circular trajectory. Such a trajectory is generated because the drop, released close to the edge of the beaker, is initially propelled almost tangentially to the wall. In Fig. 5b the drop velocity  $V(t)$  is observed to remain constant, with  $V(t) = V_A^* = 2.2 \pm 0.2 \text{ cm/s}$ .

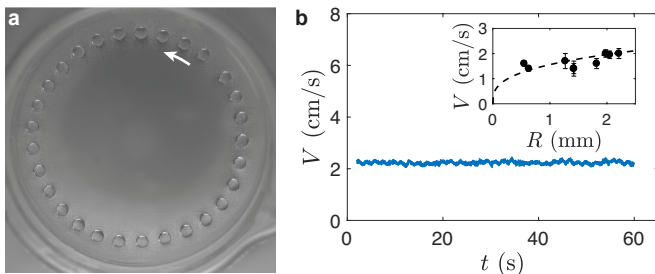


**Fig. 5.** **a.** Successive positions of a drop of liquid nitrogen with radius  $R = 1.8 \text{ mm}$  deposited close to the edge of a liquid nitrogen bath. The images are separated by 250 ms. The arrow indicates the direction of movement of the drop. Corresponding movie is Movie S7. **b.** Velocity  $V(t)$  of the liquid nitrogen drop.  $V$  stays constant, with  $V = V_A^* = 2.2 \pm 0.2 \text{ cm/s}$ . In the inset,  $V$  is plotted as a function of the drop radius  $R$ . The dotted line is a fit with  $V_A^* = 1.7 \frac{\rho g}{\eta_v} \Delta h h_{N_2}$ , with  $h_{N_2}$  as defined in Eq. 7.

Levitation of such cold objects is made possible by residual bath evaporation, happening despite the presence of an insulating box and a sacrificial bath. A 300 mL beaker with

surface  $57 \text{ cm}^2$  typically empties in 3h, which corresponds to an evaporation rate  $\dot{M} \simeq 10^{-5} \text{ kg/s}$ . This value is in close agreement to what is expected from radiative heat transfert where  $\dot{M} \sim \sigma (T_{amb}^4 - T_N^4) D^2 / L_v \simeq 2 \times 10^{-5} \text{ kg/s}$ , with  $D$  the beaker diameter,  $\sigma$  the Stefan-Boltzmann constant,  $T_{amb}$  and  $T_N$  respectively ambient and liquid nitrogen temperatures.

The continuous vapor production maintains a constantly renewed vapor film under the liquid nitrogen drops, even if the droplet itself does not transfer heat to the system. Levitating is then the same as floating above a perfectly porous substrate through which gas escapes. The film thickness  $h_{N_2}$  generated by the bath evaporation can be estimated in that situation: the vapor flux generated under the surface of a (cold) drop with radius  $R$  is  $q \sim \frac{\dot{M} R^2}{\rho_v D^2}$ . This vapor is redirected within the film, so that  $q \sim u R h_{N_2}$ , with  $u$  the mean velocity of vapor. The pressure in the film  $\Delta p$  is estimated from lubrication theory  $\Delta p \sim \eta_v R u / h_{N_2}^2$  and as the vapor film sustains the drop  $\Delta p \sim \rho g R$ . These expressions combined finally give:

$$h_{N_2} \sim \left( \frac{\eta_v \sigma (T_{amb}^4 - T_N^4) R}{\rho_v \rho g L_v} \right)^{1/3} \quad [7]$$

The measured evaporation rates yield  $h_{N_2} \simeq 10 \mu\text{m}$  which is smaller than the film thickness expected for hot drops ( $h_0 \simeq 50 \mu\text{m}$ ), but sufficient to enable levitation. Moreover, Eq. 7 predicts  $h_{N_2} \propto R^{1/3}$ , which we verified: indeed, Eq. 6, predicts that  $V_A^*$ , proportional to  $h = h_{N_2}$  here, should also vary as  $R^{1/3}$ . The velocity  $V_A^*$  of liquid nitrogen drops was measured for varying radii  $R$  (inset of Figure 5b): the dotted line shows our model with  $V_A^* = 1.7 \frac{\rho g}{\eta_v} \Delta h h_{N_2}$ , which fits reasonably well with our data, with a prefactor close to 1.

The same mechanism that enables non-coalescence of liquid nitrogen drops also causes the persistence of levitation of initially hot droplets, long after they freeze to liquid nitrogen temperatures. Indeed, from Eq. 6 and 4, one would expect the drops to sink at the end of the deceleration phase, when the film thickness  $h$  diminishes to zero. However, the bath residual evaporation - as described earlier - generates a constant vapor flux that adds up to the Leidenfrost flux. Even if this additional vapor flux is negligible in the first seconds (it is initially 100 times smaller), it becomes of critical importance as the levitating drops cool down. Indeed, it generates a  $10 \mu\text{m}$  thick vapor film (as estimated from Eq. 7), which is sufficient to maintain in levitation droplets sufficiently light and smooth.

**Full model and discussion.** To also model the dynamics of drops after they completely cool down (as in Fig. 2a), we now consider the influence of the residual vapor flux on the film thickness  $h$ . The calculation is provided in the SI Appendix: by adding the two fluxes, the film thickness  $h(t)$  is found to be the solution of a polynomial equation:  $h(t)^4 = (h_0(1 - t/\tau))^4 + h_{N_2}^3 h(t)$ , that can be solved for any time  $t$ . We solved Eq 5 numerically by taking this last element into account: the continuous lines plotted in Figures 2 and 4 show the velocity profiles predicted by the model, with fitting parameters  $\alpha = \beta = 15$  and  $\Delta h = 1.45 \mu\text{m}$ ;  $\tau$  and  $h_{N_2}$  are calculated from Eq. 4 and 7, respectively. As seen in Figure 2a, the model matches all three phases of the drop movement. It also nicely reproduces the drop dynamics for varying initial conditions (Fig. 2b), liquid nature (Fig. 2c) and drop radii

621 (Fig. 4a) without any change in the fitting parameters. This  
622 model, although simplified (it does not consider the variation  
623 of liquids properties as the droplets cool down, as well as the  
624 freezing dynamics) accounts convincingly for the details of the  
625 evolution of velocity amplitudes.

626 Remarkably, both experiments and numerical simulations  
627 are consistent with a stable symmetry breaking  $\Delta h$ , which  
628 remains constant during the drop's lifetime (even if the vapor  
629 flux diminishes by a factor 100), and which does not vary with  
630 the drop size. Even if we cannot fully explain the exceptional  
631 stability of the asymmetric state, we can provide clues on its  
632 origin. In particular, the consistent motion of non-deformable  
633 objects (frozen drops or polyethylene marbles, as in Movie S2)  
634 indicates that  $\Delta h$  most certainly originates from an asymmet-  
635 ric deformation of the liquid nitrogen interface. What could  
636 then cause the surface of the bath to deform? A hypothesis is  
637 that the symmetry breaking is generated by an instability of  
638 the morphology of the vapor film itself, which is very different  
639 from that of classical Leidenfrost drops over a flat rigid sub-  
640 strate (13, 20). In particular, a recent theoretical study (27)  
641 shows that the film exhibits localized oscillations at the neck,  
642 which can develop within the whole film for drops smaller than  
643 the capillary length. We surmise that these oscillations may  
644 be unstable, which would trigger a symmetry breaking when  
645 they are very slightly disturbed.

646 **Conclusion.** We demonstrate that drops deposited on a cold  
647 bath are naturally self-propelled, without external forcing. The  
648 complexity of drop dynamics results from the combination  
649 of three elements: i) a stable symmetry breaking (associated  
650 with a variation  $\Delta h$  of the film thickness) which causes self-  
651 propulsion ii) the thinning of the vapor film under the drops  
652 - due to their cooling - that increases the friction and is re-  
653 sponsible for their deceleration and, finally, iii) the residual  
654 evaporation of the bath, which can cause persistent levitation  
655 long after drops freeze to the bath temperature.

656 An interesting parallel can be drawn with the very recent  
657 paper of A. Bouillant *et al.* (28) who showed that small drops  
658 can also exhibit spontaneous self-propulsion on flat solids.  
659 While, on solids, motion is induced by a symmetry breaking  
660 in the internal flow of the droplets, on a bath, it is most  
661 surely generated by an instability happening at the liquid  
662 nitrogen interface. This difference fundamentally affects the  
663 behavior of the levitating objects: first, solid marbles can  
664 self-propel here and they glide without rotation. In addition,  
665 the propelling force switches direction and instantly reappears  
666 after the drops have been reflected from a wall. This can be  
667 used to control droplets trajectories with very fine precision,  
668 by confining them between two walls. We can finally note that  
669 spontaneous motion is not solely limited to cryogenic baths:  
670 liquid nitrogen drops can also self-propel on a ethanol bath (as  
671 in Movie S8). This might increase the scope of such a study  
672 to ambient temperature situations.

## 675 Materials and Methods

676 **Homemade cryostat.** The cryostat is a box of expanded  
677 polystyrene, with dimensions 30 x 30 x 25 cm and 4 cm thick walls.  
678 Inside is placed a sacrificial bath (a beaker with diameter 19 cm  
679 filled with 5 cm of liquid nitrogen). At its center, another beaker,  
680 with diameter  $D = 7.6$  cm is placed on a copper disk and filled with  
681 10 cm of liquid nitrogen. The cryostat is closed by a polystyrene  
682 lid, which is removed for each experiment and then replaced.

683 **Drops tracking.** A home-made Python algorithm is used: it  
684 automatically extracts the (x,y) position of the drop center from  
685 an initial frame with known drop position and size. Bilateral filter-  
686 ing and median-estimated background subtraction are first applied.  
687 Then, at each step the drop position is estimated (from the previ-  
688 ously tracked position and speed) and the image is cropped around  
689 it. A gaussian-blurred circle is drawn separately, and its center  
690 and radius are optimized through brute-force search to minimize its  
691 mean-squared error with the cropped image. This gives the drop  
692 location and radius with pixel precision.

692 **Numerical method.** The numerical simulation is based on a  
693 finite element method of the incompressible 2d Cartesian Navier-  
694 Stokes equations with sharp interfaces aligned with the mesh (see  
695 SI Appendix for more details). The two-dimensional simulation  
696 domain has a size of 77 mm x 45 mm. The liquid surface is placed  
697 at a height of 20 mm, with a contact angle of 20° with respect  
698 to the walls. The implementation is done using the framework  
699 OOMPH-LIB.(29).

700 **ACKNOWLEDGMENTS.** The authors warmly thank Dominic  
701 Vella for insightful comments on the model, Corentin Tregouet for  
702 his initial and fruitful theoretical input and Guillaume Lajoinie for  
703 carefully reading the manuscript.

1. J. Leidenfrost (1756) De aquae communis nonnullis qualitatibus tractatus. *Ovenius*.
2. A.-L. Bianco, C. Clanet & D. Quéré (2003) Leidenfrost drops. *Phys. Fluids*, **15**(6):1632-1637.
3. T. Tran, H. Staat, A. Prosperetti, C. Sun & D. Lohse. (2012) Drop impact on superheated surfaces. *Phys. Rev. Lett.* **108** 036101.
4. F. Celestini, T. Frisch & Y. Pomeau. (2012) Take-off of small Leidenfrost droplets. *Phys. Rev. Lett.* **109** 034501.
5. P. Brunet and J. Snoeijer. (2011) Star-drops formed by periodic excitation of an air cushion: a short review. *Eur. Phys. J. Spec. Top.* **192** 207-226.
6. D. Quéré (2013) Leidenfrost dynamics. *Annu. Rev. Fluid Mech.* **45** 197-215.
7. H. Linke, B. Alemán, L. Mellinger, M. Taormina, M. Francis, C. Dow-Hygelund, V. Narayanan, R. Taylor & A. Stout. (2006) Self-propelled Leidenfrost droplets. *Phys. Rev. Lett.* **96**(15):154502.
8. G. Dupeux, M. Le Merrer, G. Lagubeau, C. Clanet, S. Hardt & D. Quéré. (2011) Viscous mechanism for Leidenfrost propulsion on a ratchet. *Europhys. Lett.* **96**(5):58001.
9. T. Cousins, R. Goldstein, J. Jaworski & A. Pesci. (2012) A ratchet trap for Leidenfrost drops. *J. Fluid Mech.* **696**:215-227.
10. Á.G. Marín, D.A. del Cerro, G.R.B.E. Römer, B. Pathiraj, A.H. in't Veld and D. Lohse. (2012) Capillary droplets on Leidenfrost micro-ratchets. *Phys. Fluids* **24**(12):122001.
11. D. Soto, G. Lagubeau, C. Clanet, C & D. Quéré. (2016) Surfing on a herringbone. *Phys. Rev. Fluids* **1**(1): 013902.
12. A. Hashmi, Y. Xu, B. Coder, P. Osborne, J. Spafford, G. Michael, G. Yu & J. Xu. (2012) Leidenfrost levitation: beyond droplets. *Sci. Rep.* **2**:797.
13. L. Maquet, B. Sobac, B. Darbois-Texier, A. Duchesne, M. Brandenbourger, A. Rednikov, P. Colinet, & S. Dorbolo. (2016) Leidenfrost drops on a heated liquid pool. *Phys. Rev. Fluids* **1**(5):053902.
14. A. Snezhko, E. Ben Jacob, and I. Aranson (2008) Pulsating-gliding transition in the dynamics of levitating liquid nitrogen droplets. *New J. Phys.* **10**(4):043034.
15. H. Kim, Y. Lee and H. Cho (2011) Levitation time measurement of water drops on the surface of liquid nitrogen *J. Korean Phys. Soc.* **58**(6):1628-1632.
16. M. Adda-Bedia, S. Kumar, F. Lechenault, S. Moulinet, M. Schillaci & D. Vella. (2016) Inverse Leidenfrost effect: Levitating drops on liquid Nitrogen. *Langmuir* **32**(17):4179-4188.
17. S. Wildeman, S. Sterl, C. Sun, & D. Lohse. (2017) Fast dynamics of water droplets freezing from the outside in. *Phys. Rev. Lett.* **118**(8):084101.
18. S. Janssens, S. Koizumi & E. Fried. (2017) Behavior of self-propelled acetone droplets in a Leidenfrost state on liquid substrates. *Phys. Fluids* **29**:032103.
19. D. Vella (2015) Floating versus sinking. *Annu. Rev. Fluid Mech.* **47**:115-135.
20. C. Wong, M. Adda-Bedia & D. Vella (2017) Non-wetting drops at liquid interfaces: From liquid marbles to Leidenfrost drops. *Soft Matter* **13**:5250-5260.
21. I. Vakarelski, J. Marston, D. Chan, S. Thoroddsen. (2011) Drag reduction by Leidenfrost vapor layers. *Phys. Rev. Lett.* **106**(21):214501.
22. M. Le Merrer, C. Clanet, D. Quéré, Élie Raphaël, and Frédéric Chevy (2011) Wave drag on floating bodies. *Proc. Natl. Acad. Sci. USA* **108**(37):15064-15068.
23. Y. Song, D. Adler, F. Xu, E. Kayaalp, A. Nureddin, R. Anchan, R. Maas & U. Demirci. (2010) Vitrification and levitation of a liquid droplet on liquid nitrogen. *Proc. Natl. Acad. Sci. USA* **107**(10):4596-4600.
24. H. Feng, Y. Xu, & T. Yang. (2018) Study on Leidenfrost effect of cryoprotectant droplets on liquid nitrogen with IR imaging technology and non isothermal crystallization kinetics model *Int. J. Heat Mass Transfer* **127**:413-421.
25. R.S. Hall, S. Board, A. Clare, R. Duffey, T. Playle & D. Poole. (1969) Inverse leidenfrost phenomenon. *Nature* **224**:5216.
26. G. Dupeux, T. Baier, V. Bacot, S. Hardt, C. Clanet & D. Quéré. (2013) Self-propelling uneven Leidenfrost solids. *Phys. Fluids* **25**(5):051704.
27. M. van Limbeek, B. Sobac, A. Rednikov, P. Colinet, P & J. Snoeijer. (2018) Asymptotic theory for a Leidenfrost drop on a liquid pool. *arXiv preprint arXiv:1805.12003*.
28. A. Bouillant, T. Mouterde, P. Bourriane, A. Lagarde, C. Clanet & D. Quéré. (2018) Leidenfrost wheels *Nat. Physics* **14**:1188-1192.
29. M. Heil & A. L. Hazel (2006) oomph-lib – an object-oriented multi-physics finite-element library. *Fluid-Structure Interaction* **53**:19-49